Check for updates

Graphene oxide prevents lateral amygdala dysfunctional synaptic plasticity and reverts long lasting anxiety behavior in rats

Audrey Franceschi Biagioni [a,1], Giada Cellot [a,1], Elisa Pati [a], Neus Lozano [b], Belén Ballesteros [b], Raffaele Casani [a], Norberto Cysne Coimbra [c], Kostas Kostarelos [b,d], Laura Ballerini [a,*]

[a] Neuron Physiology and Technology Lab, International School for Advanced Studies (SISSA), Neuroscience, Via Bonomea 265, 34136, Trieste, Italy
[b] Catalan Institute of Nanoscience and Nanotechnology (ICN2), CSIC and BIST, Campus UAB, Bellaterra, 08193, Barcelona, Spain
[c] Laboratory of Neuroanatomy & Neuropsychobiology, Department of Pharmacology, Ribeirão Preto Medical School of the University of São Paulo (FMRP-USP), Av. Bandeirantes 3900, 14049-900, Ribeirão Preto, SP, Brazil
[d] Nanomedicine Lab, National Graphene Institute and Faculty of Biology, Medicine & Health, The University of Manchester, AV Hill Building, Oxford Rd, Manchester, M13 9PL, United Kingdom

ARTICLE INFO

ABSTRACT

Engineered small graphene oxide (s-GO) sheets were previously shown to reversibly down-regulate glutamatergic synapses in the hippocampus of juvenile rats, disclosing an unexpected translational potential of these nanomaterials to target selective synapses _in vivo_. Synapses are anatomical specializations acting in the Central Nervous System (CNS) as functional interfaces among neurons. Dynamic changes in synaptic function, named synaptic plasticity, are crucial to learning and memory. More recently, pathological mechanisms involving dysfunctional synaptic plasticity were implicated in several brain diseases, from dementia to anxiety disorders. Hyper-excitability of glutamatergic neurons in the lateral nucleus of the amygdala complex (LA) is substantially involved in the storage of aversive memory induced by stressful events enabling post-traumatic stress disorder (PTSD). Here we translated in PTSD animal model the ability of s-GO, when stereotaxically administered to hamper LA glutamatergic transmission and to prevent the behavioral response featured in long-term aversive memory. We propose that s-GO, by interference with glutamatergic plasticity, impair LA-dependent memory retrieval related to PTSD.

1. Introduction

Emerging evidence in mammals indicates the amygdala complex as the brain structure implicated in the development of anxiety disorder [1–3]. In animal models, core behavior related to anxiety can be induced by responses to fear stimuli [4,5] and previous elegant experiments suggested that the over-activation of distinct populations of basal amygdala neurons, such as glutamatergic ones effectively sustain fear behavior [6–8]. Moreover, dysfunctions in the glutamatergic system have a primary role in several brain diseases [9] and severe mood disorders are increasingly associated to altered synaptic plasticity [10]. In such a context, the glutamatergic system, known to play a major role in tuning neuronal plasticity [11,12], may represent a promising target to treat pathologies involving alterations in excitatory neurotransmission.

New biotechnology-based therapeutic interventions for brain pathologies have involved engineering of novel nanomaterials, such as graphene, the one carbon atom thick 2-dimensional (2D) material [13]. Graphene or its derivatives such as its oxide form, graphene oxide (GO), have been exploited as components of bioelectronic devices, as (nano) vectors in drug-delivery platforms and engineered as promising tissue scaffolds [14–17]. We have previously shown the ability of small graphene oxide nanosheets (s-GO), to transiently impair glutamatergic transmission in the rat hippocampus, both _in vitro_ and _in vivo_, presumably with a direct interference with the presynaptic glutamate release machinery [18]. More recently, additional studies sustained s-GO synapse specificity and kinetics when injected in specific Central Nervous

System (CNS) areas and further showed in zebrafish larvae *in vivo* that s-GO injected directly to the spinal cord were able to reduce glutamatergic transmission, effectively impairing locomotor behavior [19]. In the current work, a rat model of an anxiety disorder (post-traumatic stress disorder (PTSD)) was established, and a suspension of thin s-GO nanosheets was administered in a single dose in the LA to prevent pathological long-term enhancement in excitatory neurotransmission. Behavioral studies combined with tissue histology, confocal microscopy and *ex vivo* electrophysiology, demonstrated that s-GO sheets were able to block LA glutamatergic synaptic plasticity *in vitro*, to impair long-term aversive memory and long-lasting anxiety-related responses *in vivo*.

2. Material and methods

2.1. Graphene oxide material synthesis and characterization

s-GO solution was prepared by the modified Hummers' method as previously described [20], using graphite powder (Sigma-Aldrich) as a starting material [21] and under endotoxin-free conditions [22]. The physicochemical characterization of the s-GO sheets was performed as previously described [23] and is summarized in Table S1.

Scanning electron microscopy (SEM) was performed using a FEI Magellan 400 L XHR SE microscope equipped with a newly developed electron column with a monochromator, UC (UniColore) Technology. Landing energy of 20.00 kV and beam current of 0.10 nA were used and signal was acquired with secondary electrons through-lens detector (TLD). 20 μL of s-GO solution at 100 μg/mL were deposited on an ultrathin carbon film on lacey carbon TEM grid and dried for at least 24 h. Lateral dimension distribution was performed by manual counting of the longest sheet dimension on Image J software. The oxidation of the material has been studied by several techniques such as Raman spectroscopy, surface charge (ζ-potential) measurements, TGA and XPS analysis (Table S1).

Animals, overall experimental design and surgery: All experimental procedures were carried out in accordance with the Italian law (decree 26/14) and the EU guidelines (2007/526/CE and 2010/63/UE) and were approved by the Italian Ministry of Health (n. 689/2017-PR). Male adult Wistar rats weighed 230–250 g (n = 60) were used to perform the *in vivo* experiments. Food and water were provided at libitum. The enclosure was maintained at 20 ± 2 °C on a light-dark cycle (lights on from 7 a.m. to 7 p.m.). Behavioral experiments were performed between 9 a.m. and 2 p.m. Rats undergoing surgical procedures were deeply anaesthetized. Analgesic and antibiotic medications were administrated postoperatively. All experimental procedures were planned to minimize the number of animals used and their suffering. We evaluated the aversive memory by the odor avoidance box, which consisted of a rectangular arena (40 × 26 × 36 cm) with black acrylic-plexiglass walls covered with a transparent plexiglass lid. At one side of the arena, an alligator clip fixed in the wall is positioned 4 cm above the floor. In the opposite direction, a smaller box (20 × 26 × 22 cm) covered with a black plexiglass lid is positioned, named hide box. The arena and the hide box were separated by a small 6 × 6 cm square hole allowing free access to both chambers. Rats were placed (10 min) inside the hide box with free access to the arena for 3 consecutive days to habituate to the apparatus. On the fourth day, the time spent in the following defensive behavior was recorded: head out (namely, the rat scanning the environment from a protected position, measured as poking of the head, or of head and shoulders, outside of the hide box but with the bulk of the rat body inside of it). Rats were divided in two groups (n = 6 per group), exposed to a piece (2 cm) of an unworn collar (UC), without any cat odor, and the group exposed to the collar previously worn by the cat, named worn collar (WC). Collars were worn by an encaged cat. Rats were re-exposed (10 min) to the context, arena without the cat collar to evaluate the aversive memory related to the conditioned fear. Behaviors were analyzed during the re-exposure to the context at 2 days and 6 days post-exposure. Long-term anxiety-related behavior was measured using the

elevated plus maze (EPM). This apparatus consisted of four arms (50 × 10 × 40 cm), two open arms (without walls) and two closed arms (with 40 cm high walls) connected by a central square (10 × 10 cm). The maze was elevated 50 cm from the ground. Rats (n = 6 per group) were placed in the closed arm and were allowed to freely explore the apparatus for 5 min. Duration and frequency of entrance in the open and closed zone was evaluated. Entry into a zone was scored when the center-point of the rat's body was within it. We adopted an *anxiety index* which was previously validated [24] and calculated for each rat based on the EPM behavioral scores. In this scoring system, high anxiety index values represent an elevated anxiety-like behavior expression. The following formula was applied:

anxiety index = 1- [(time spent in the open arms/ total time in the maze) + (number of entries to the open arms/ total time of maze exploration)]/2.

Exploratory and locomotor activities of rats (n = 6 per group) were measured by the open field (OF) apparatus, a square arena with the 60 × 60 cm transparent plexiglass walls and the floor divided into 16 sections (15 × 15 cm). Number of crossings (considered when the rat crossed the border line of each section with four paws) were analyzed following the EPM testing. All behavioral tests were performed under 40 lx luminosity and videorecorded for off-line analysis. The XPloRat software [25] was used to score the behaviors. Animals were anaesthetized with intraperitoneal injection of ketamine (Ketamine Imalgene®, Merial Laboratories) and xylazine (Sedaxylan®, Dechra Veterinary Products) at 92 mg/kg and 10 mg/kg body weight, respectively, and fixed in a stereotaxic frame. A stainless-steel guide cannula (outer diameter, 0.6 mm, and inner diameter, 0.4 mm) was implanted in the diencephalon aimed to the LA. The upper incisor bar was set at 3.3 mm below the interaural line so that the skull was horizontal between bregma and lambda. The guide cannula was vertically introduced using bregma as the reference and the following coordinates: A.P.−3.48 mm, M.L.−5.2 mm and D.V.−7 mm, according to Ref. [26]. At the end of the surgery, the acrylic resin and two stainless steel screws were used to fix the guide cannula in the skull. In order to protect the guide cannula from obstruction a stainless-steel wire was used to seal it. Three days later, rats were gently wrapped in a cloth and held while they received a random treatment into LA of either s-GO (50 μg/mL) or ACSF solution (composition described below) delivered by a needle (0.3 mm of outer diameter) linked to a syringe (Hamilton) through a polyethylene tube. The injection needle was inserted through the guide-cannula until it reached the LA (1 mm below the guide-cannula). 48 h later animals were submitted to the behavioral testing.

2.2. Histology, microscopy and image analysis

Rats were anaesthetized as described above and submitted to the transcardial perfusion with 0.1 M PBS followed by 4% formaldehyde (prepared from fresh paraformaldehyde; PFA, Sigma, St Louis, MO, USA) in PBS. The brain was removed from the skull and prepared as described previously [27]. Briefly, brains were post fixed, cryoprotected, frozen on dry-ice and sectioned on a cryostat (Microm HM 550, Thermo Fisher Scientific). The brain slices (30 μm coronal sections) were mounted on glass slides and processed according to either cresyl violet staining or immunohistochemical methods. Brain slices were stained in 0.1% cresyl violet (Sigma) solution for 5 min, rinsed in distilled water twice for 2 min each wash and dehydrated in a graded ethyl alcohol series: 50%, 70%, 95% and 100%. Thereafter, they were cleared in xylene for 3 min and mounted with Permount (Fisher Scientific). Histological sections were analyzed and images were acquired using a Leica DM6000 upright microscope with a 2.5 × dry objective. Alternatively, brain slices were washed out with 0.1 M PBS, incubated with a blocking solution composed of 3% BSA, 3% FBS, and 0.3% Triton X-100 in PBS for 45 min at room temperature (RT). The primary antibodies anti-ionized calcium-binding adaptor molecule 1 (Iba1; Wako, specific marker for

microglia, 1:500) and mouse anti-glial fibrillary acidic protein (GFAP; Sigma-Aldrich, specific marker for glial cells, 1:400, diluted in saline and 5% fetal bovine serum), were incubated overnight. Sections were washed 3 times for 5 min each, incubated with the secondary antibodies (1:400) AlexaFluor 488 goat anti-mouse (Thermo Fisher Scientific) and AlexaFluor 594 goat anti-rabbit, (Thermo Fisher Scientific), for 3 h in the dark and washed. Nuclei were labeled with DAPI (Invitron, 1:500) in PBS for 25 min at RT. All slides were cover slipped Fluoromounting [18].

Using a Nikon A1R confocal microscope, equipped with argon/krypton, helium/neon, and UV lasers images were acquired with a 40 × (1.2 NA) objective and confocal sections were acquired every 0.5 μm up to a total Z-stack thickness of 20 μm. Gain, pixel-resolution, and exposure time remained constant for all images. From each section, we selected six regions of interest (ROI, 320 × 320 μm^2), where the cell densities of Iba1 and GFAP positive cells were calculated and normalized for those of the contralateral hemisphere. In order to investigate the presence of s-GO in the LA 48 h after injection, the same brain slices immunolabelled for DAPI, GFAP and Iba1 were visualized using the reflection mode property during the confocal acquisition [28] at 40 × (1.2 NA) with ROI of 140.77 × 140.77 μm^2.

Image analysis was performed using Volocity software (Volocity 3D image analysis software, PerkinElmer, U.S.A.).

2.3. Immunohistochemistry and golgi-staining and quantification of dendritic spines

After behavioral experiments, a group of rats (n = 8) re-exposed to the context (6 days) were anaesthetized as described above and decapitated, their brains were collected and prepared to the Golgi-Cox staining protocol [29]. Briefly, brains were incubated in the Golgi-Cox solution (1% potassium dichromate, 0.8% potassium chromate and 1% mercuric chloride) in the dark at RT for 25 days. After that, brains were incubated in sucrose solution at 30% for 24 h and sectioned in coronal sections (400 μm thickness) at the level of the amygdala using a vibratome (Leica VT100S). Brain slices were mounted onto microscope slides with Permount (Fisher Scientific). Histological sections were analyzed and images stacks of the LA neurons were acquired using a Leica DM6000 upright microscope with a 63 × oil immersion objective. The serial section images were aligned and dendritic spines of pyramidal neurons were blind analyzed [30] in RECONSTRUCT software (http://synapses.clm.utexas.edu/tools/reconstruct/reconstruct.stm; RID: SCR_002716). Dendrite originating directly from the cell body with a length of 70 μm from its origin was analyzed [31,32]. All dendrite protrusions were considered as spines, regardless to their morphological characteristics.

2.4. In vitro amygdala preparations

All experimental procedures were carried out in accordance with the Italian law (decree 26/14) and the EU guidelines (2007/526/CE and 2010/63/UE) and were approved by the Italian Ministry of Health (n. 689/2017-PR, n. 22DAB.N.1Z8 and n. 22DAB.N.1WO). For acute slices male P12–P16 juvenile Wistar rats (n = 17) were used. Briefly, after being decapitated, the brain was quickly removed from the skull and placed in ice-cold solution containing (in mM): sucrose 215, KCl 3.5, NaH$_2$PO$_4$ 1.2, NaHCO$_3$ 25, CaCl$_2$ 2, MgCl$_2$ 1.3, glucose 25 and ascorbic acid 4, saturated with 95% O$_2$–5% CO$_2$ (pH 7.3–7.4). Coronal amygdalar slices (300 μm thick) were cut with a vibratome (LeicaVT1000S) and stored at room temperature in a holding bath containing 130 mM NaCl instead of sucrose that was gassed with 95% O$_2$–5% CO$_2$ (artificial cerebrospinal fluid solution, ACSF).

For cultures, postnatal P7-10 Wistar rats were used. Dissociated amygdalar cultures were prepared as previously described [33]. Briefly, brains were quickly removed and cut in coronal sections (400 μm thickness) using a vibratome (Leica VT100S). Three sections at the level of the amygdalar complex were collected using the following

coordinates: Bregma −1.8 mm, −2.4 mm and 2.8 mm [34]. From these, the amygdaloid complex was visually identified under a dissection microscope and dissected using a biopsy punch. The collected tissue was enzymatically and mechanically dissociated and cells were seeded onto poly-L-ornithine-coated glass coverslips at a density of 800 cells/mm^2 and maintained in controlled conditions (at 37 °C, 5% CO2) for 8–12 days prior to voltage-clamp recordings.

2.5. s-GO treatments in vitro

Acute slices were incubated for 5 h with 50 μg/mL of s-GO, added directly to the ACSF, and as control, sister slices were kept in ACSF alone (saline-treated). At the end of incubation time, an individual slice was transferred to a submerged recording chamber and continuously perfused at 33–34 °C with ACSF. In the experiments in which s-GO were applied acutely, a gravity driven perfusion system was used and a solution of 10 μg/mL s-GO was applied at a speed of 2 mL/min for 5 min. In the experiments on dissociated cultures, s-GO were applied at a concentration of 20 μg/mL for 30 s through the perfusion system in combination with 50 μM of glutamate.

2.6. Electrophysiology

Patch clamp whole-cell recordings were obtained with glass pipettes (resistance 5–7 MΩ) filled with the following solution (in mM) 120 K gluconate, 20 KCl, 10 HEPES, 10 EGTA, 2 MgCl$_2$, 2 Na$_2$ATP (pH 7.3, osmolarity adjusted to 300 mOsm). The extracellular solution was ACSF for acute slices, and for dissociated cultures, the following saline solution (in mM): 150 NaCl, 4 KCl, 2 CaCl$_2$, 1 MgCl$_2$, 10 HEPES, 10 glucose, pH 7.4. Principal neurons of the lateral amygdala were visually identified thanks to their typical pyramidal shape [35] with an upright microscope (Eclipse FN1; Nikon, Japan) equipped with differential interference contrast optics and digital videocamera (Nikon, Japan). Data were collected by Multiclamp 700 A patch amplifier (Axon CNS, Molecular Devices) and digitized at 10 KHz with the pClamp 10.6 acquisition-software (Molecular Devices LLC, USA). Membrane potential values were not corrected for the liquid junction potential that was of ~15 mV (calculated with the Clampex software; Molecular Devices, Sunnyvale, CA, USA). The stability of the patch was checked by repetitively monitoring the input and series resistance during the experiments. Cells exhibiting 15% changes were excluded from the analysis. The series resistance was <20 MΩ and it was not compensated. Input resistance and cells capacitance were measured online with the membrane test feature of the pClamp software. In pyramidal neurons in the LA slices, cell capacitance, input resistance and resting membrane potential did not show any statistically significant difference between in s-GO treated and saline treated neurons (p > 0.05, Table S2).

In current clamp experiments, 1 s long lasting steps of positive current with increasing amplitude (10, 20, 30, 40, 50, 60, 70, 80, 90, 100 pA) were injected in pyramidal cells from a resting membrane potential of −65 mV. Both s-GO-treated and untreated neurons showed comparable firing properties (Fig. 4C), measured as threshold for action potential, amount of injected current needed to reach it and action potential amplitudes. No statistically significant differences were observed between the two groups (p > 0.05, Table S2).

In the experiments where slices were chronically incubated in s-GO, the glutamatergic synaptic activity was recorded at a holding potential of - 65 mV, in the presence of gabazine (10 μM; a blocker of GABA$_A$ receptor mediated postsynaptic currents). EPSCs were collected from traces and averaged (showed in Fig. 4F) and no differences were observed in their amplitude (in saline-treated neurons: 9 ± 1 pA and in s-GO-treated ones: 8 ± 2 pA), rise time (in saline-treated neurons: 1.2 ± 0.2 ms and in s-GO-treated ones: 1.1 ± 0.1 ms) and decay time constant τ (in saline-treated neurons: 5.4 ± 0.9 ms and in s-GO-treated ones: 4.7 ± 0.4 ms) when incubated with s-GO (n = 8 cells) in respect to control (n = 9 cells; p > 0.05). After recording spontaneous activity for 8 min as

baseline, LTP was induced in dissociated cultures by applying 50 μM of glutamate for 30 s, while the membrane potential of the recorded cell was depolarized from −58 mV to +4 mV (under voltage clamp mode). The effects of LTP induction were monitored for 30 min by measuring EPSC and IPSC frequencies and amplitudes. The values reported are averages calculated between 24 and 30 min after LTP induction and normalized for the pre-treatment baseline values. In the experiments of s-GO application through the perfusion system in acute slices and in dissociated cultures, sPSCs were recorded in the absence of any drugs and were analyzed offline using the software AxoGraph X (Axograph Scientific), which exploits a detection algorithm based on a sliding templates to separate EPSCs and IPSCs on the basis of their different decay times (see Results). For each recording, events were collected and averaged to measure the peak amplitude and kinetic properties on the resulting trace. The decay time of PSCs was calculated by fitting the decaying phase of the current with a mono-exponential function. In paired recordings, the presynaptic neuron in current clamp mode was held at −70 mV (by ≤ 0.02 nA negative current injection), and action potentials were evoked by delivering short (4 ms) positive (1 nA) square current pulses. Monosynaptic connections were identified by their short delay (<3 ms) [18], measured between the peak of the evoked action potential and the onset of the unitary evoked PSCs. Recordings of EPSCs and IPSCs at different holding potentials were used to extrapolate I/V curves (Supplementary Figure S2).

2.7. Data analysis and statistics

Data from independent groups of animals exposed to the cat collar were checked for normality and homogeneity and analyzed using Student's unpaired two-tailed *t*-test. All comparisons between more than 2 or 3 groups were made with one-way ANOVA and two-way ANOVAs, respectively, followed by Bonferroni post hoc test. For electrophysiological data, Shapiro-Wilk normality test was applied to evaluate the statistical distribution of the data sets. Statistically significant difference between two data sets was assessed by one-way ANOVA (if distributed as a Gaussian distribution) or by Mann–Whitney test (if not). In experiments obtained from dissociated amygdalar cells, for parametric data, the statistically significant difference among the three groups was assessed through one-way ANOVA, using Holm-Sidak's multiple comparisons test for post hoc analysis. Not parametric data were analyzed with Kruskal-Wallis test and post hoc analysis was done with Dunn's multiple comparison test. All values are expressed as mean ± SEM. P-value < 0.05 was considered statistically significant and n is the number of animals if not otherwise stated.

3. Results

The produced biology-grade s-GO dispersion [18] was characterized by AFM and SEM; in both measures s-GO flakes displayed a similar range of lateral dimensions: 0.06–1.7 μm by AFM (Fig. 1A and B) and 0.10–2.0 μm by SEM (Fig. 1D and E). Fig. 1C shows s-GO thickness, that ranged between 1 and 1.5 nm in accordance with single or few-layer sheets. The oxidation of the material was analyzed by Raman spectroscopy, surface charge (ζ-potential) measurements, TGA and XPS analysis, these measures are summarized in Table S1.

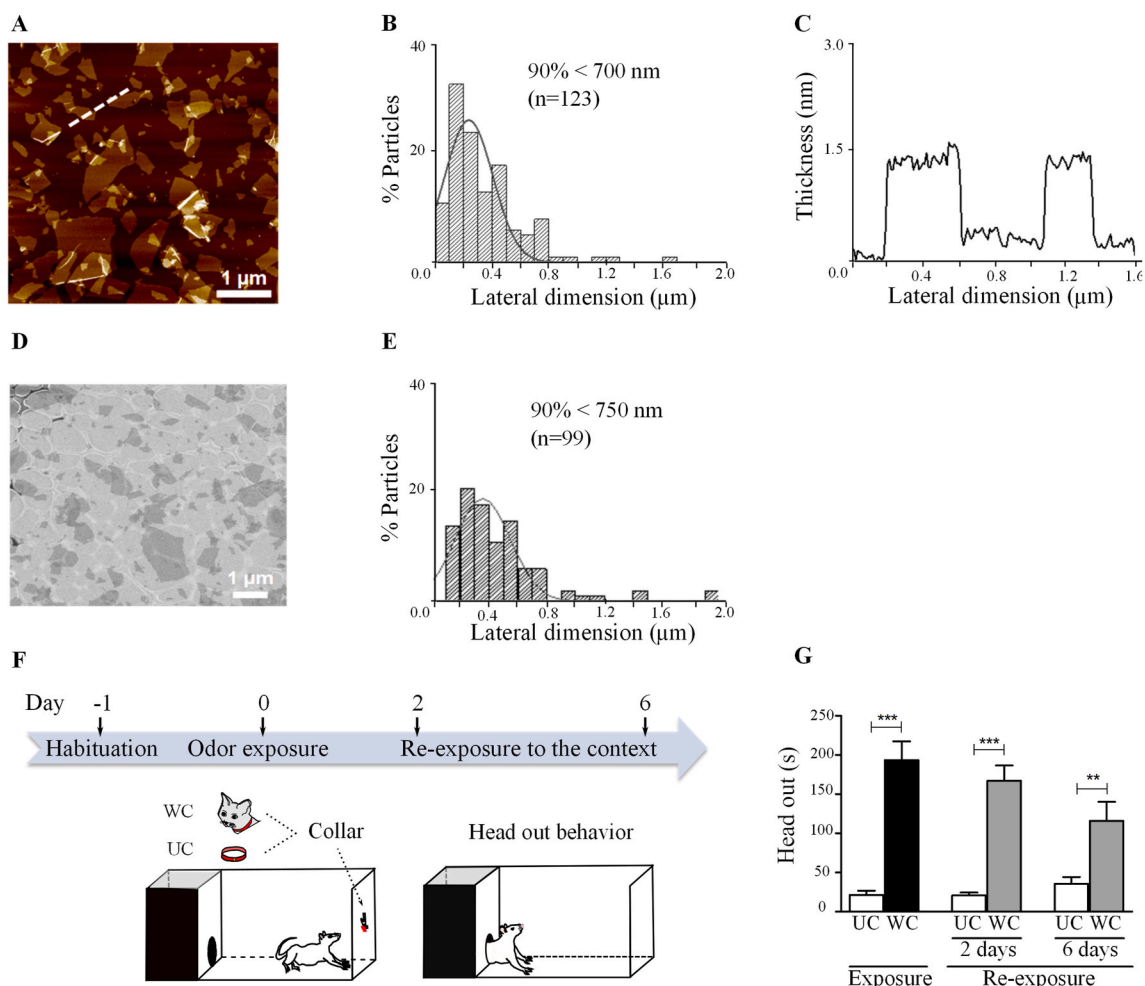Structural and morphological characterization of s-GO sheets by

Fig. 1. s-GO AFM and SEM features and the behavioral model of short- and long-term fear memories induced by aversive olfactory stimulus.

AFM: (A) height image; (B) lateral dimension distribution (based on 123 sheets); (C) cross section analysis highlighted by the dashed line in the height image; and by SEM: (D) micrograph; (E) lateral dimension distribution (based on 99 sheets). (F) Sketched experimental settings and timeline. Upon habituation in the avoidance box, adult rats were exposed to either worn (WC) or unworn (UC) cat collar. 2 and 6 days after the exposure, rats were re-exposed to the context. (G) Bar plots summarize the increase in the time of head out defensive response in rats caused by either the cat odor exposure or the re-exposure to the context 2 or 6 days later, namely short- and long-term aversive memory, respectively. N = 6 each group. ***p < 0.001; **p < 0.01 versus UC groups.

To test thin s-GO efficacy to affect neurotransmission in the LA, preventing excitatory synapses reinforcement and anxiety disorders, we established a model of PTSD upon rat exposure to an aversive stimulus, the predator (cat) odor, known to activate the amygdaloid complex [36, 37]. Such a treatment leads to hyperexcitability of LA circuits, fear responses and altered behavior [38,39]. In adult rats, immediate innate fear response was induced by single experience of an aversive (predator) olfactory stimulus and the emergence of long-lasting specific anxiety behavior was evaluated by re-exposure to the context. We adopted an

odor avoidance box (sketched in Fig. 1F) to quantify the emergence of defensive behavior ("head out" [40]; see methods). We compared defensive behavior in two groups of rats, one group exposed to a cat-worn collar (WC; n = 12) and a control group exposed to an unworn collar (UC; n = 12). In Fig. 1G the bar plots show the significant (t (10) = 7.01, p < 0.001) increase in "head out" behavior when comparing WC with UC exposed animals. The avoidance fear response was also significantly increased when comparing UC with WC groups re-exposed to the context after 2 days (t (10) = 7.46, p < 0.001) and after 6 days (t (10) = 3.13, p < 0.01), suggesting the induction of short- and long-term aversive memories, related to PTSD emergence [41,42]. The emergence of PTSD has been associated to augmented dendritic spines in the amygdala nuclei [31,32]. This anatomical signature of synaptic plasticity was confirmed in the amygdala of WC groups (6 days after first exposure, n = 4) where the number of dendritic spines in LA was significantly (p < 0.05) higher when compared to UC groups (n = 4; Supplementary Figure S1).

3.1. s-GOs locally delivered in the LA impair long-term fear memories

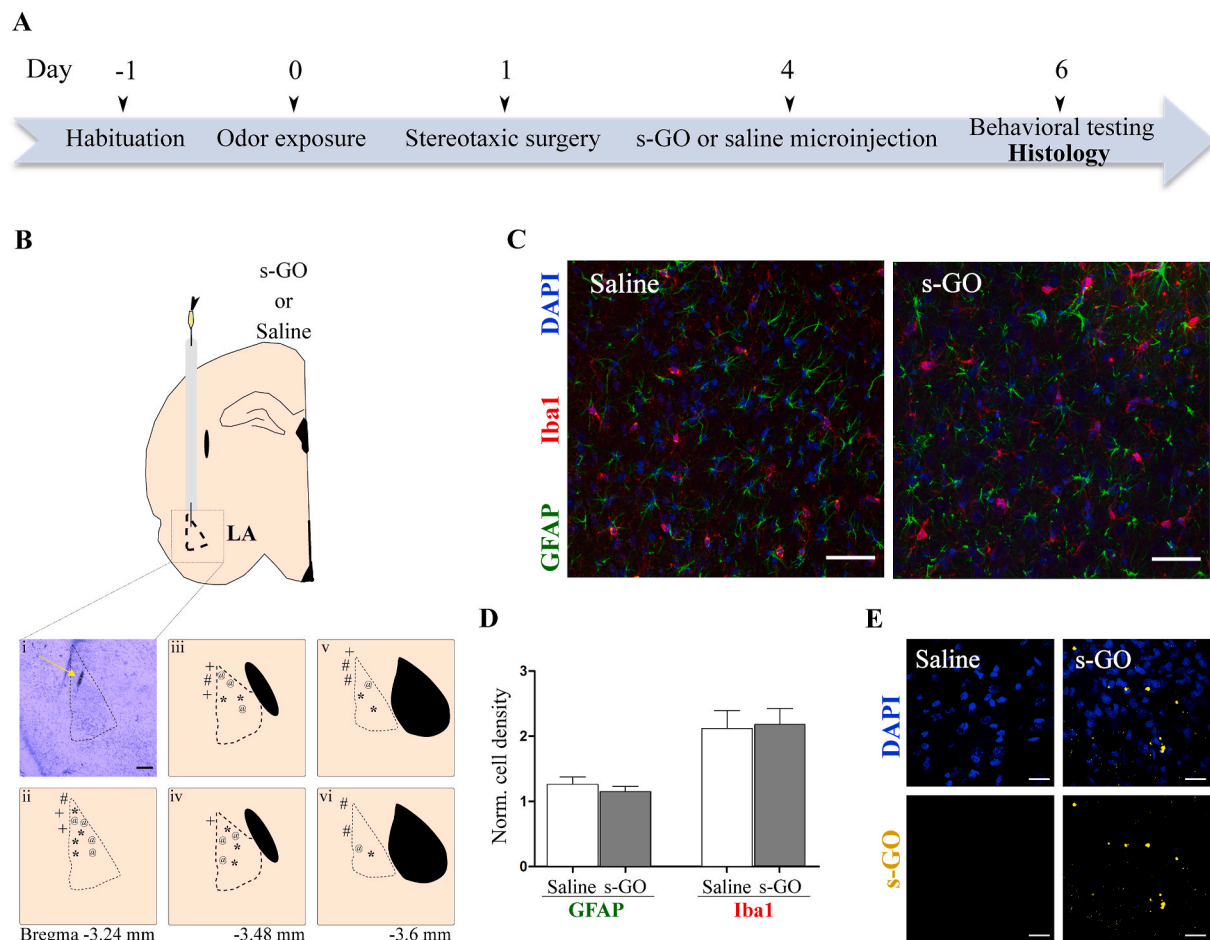The contextual avoidance behavior to predatory odor is ultimately

Fig. 2. Lateral amygdala (LA) treatment by s-GO local injection. (A) Schematic representation of experimental timeline showing the sequence of the experimental procedures, from habituation to stereotaxic surgery and histology. (B) Top, diagram of the rat brain showing the target area for s-GO or saline microinjections. Bottom, (i) representative photomicrograph of Nissl-staining (yellow arrow indicates the site of s-GO injection); scale bar 300 μm. In (ii, iii, iv, v, vi) schematic drawings of rat brain sections summarizing the microinjection points of either s-GO (* when in the LA, # when in the perirhinal cortex) or saline (@ when in the LA, + when in the perirhinal cortex). Each symbol represents an independent experiment made on a single rat. (C) Confocal photomicrographs showing GFAP- (green), Iba1- (red) reactivity and DAPI- (blue) stained nuclei in the LA slices of rats treated with either saline (left) or s-GO (right). (D) The bar plot summarizes the tissue responses in saline or s-GO treatments, N = 6 slices each group. *p > 0.05 according to the unpaired t-test. Scale bar 50 μm. (E) Representative images of LA slices (48 h after injection; same samples as in C, different fields) with DAPI (in blue) and s-GO sheets (in yellow) visualized by the reflection mode of the confocal system. Note that s-GO is visible as aggregates only in s-GO injected animals. Scale bar 20 μm. (For interpretation of the references to colour in this figure legend, the reader is referred to the Web version of this article.)

organized by the LA glutamatergic neurons [43]. We tested the hypothesis that s-GO injection into the LA, *via* transient impairment of glutamatergic synapses [18], may prevent PTSD-related behavior emergence in rodents. Such an effect would fortify the strategy of selective and transient targeting of synapses to prevent the development of brain pathologies.

Two independent groups of rats (n = 36) were exposed to WC or UC context and, after 24 h, a guided cannula was stereotaxically implanted into the rat brain, targeting the LA or, alternatively, the perirhinal cortex, to deliver locally, three days later, either s-GO (50 μg/mL) [18] or the vehicle (saline solution). Two days after s-GO or saline delivery, WC and UC groups of animals were re-exposed to the context (i.e. 6 days after the first exposure) and then euthanized (sketched in Fig. 2A). The position of the cannula was confirmed histologically in all animals both when targeting the LA and when targeting the perirhinal cortex, a neighboring brain structure (see Methods, schematic drawings and histology of Fig. 2B). Tissue reactivity was studied by immunofluorescence assessment of GFAP-positive astrocytes and Iba1-positive microglia. At 6 days post-surgery, tissue reactivity was comparable in the two animal groups, saline or s-GO treated (Fig. 2C and bar plot in D).

We tested the presence of s-GO within the LA (48 h post-injection) by operating the confocal microscopy under reflection mode, which allows the visualization of s-GO [28]. Fig. 2E shows confocal reconstructions of saline and s-GO treated LA, in the latter residual aggregates of s-GO (in yellow, reflection mode) were detected, confirming our previous observations on the duration of s-GO permanence once injected in the adult brain [18].

In all animals, aversive behavior prior to surgery was quantified and the avoidance response was significantly higher in the WC group when compared to UC one (t (10) = 4.09, p < 0.05; Fig. 3A and B). We then analyzed long-term aversive memory related behavior at day 6, namely

2 days after delivery of s-GO or saline in WC and UC groups. During the re-exposure to the stress-related context, in LA saline-treated animals, we detected the expected (see also Fig. 1G) significant increase in the "head out" response in WC (F (1,20) = 0.04, p < 0.001) when compared to UC group. Remarkably, in LA s-GO-treated animals, flakes injection reversed the long-term conditioned fear reaction in WC (F (1,20) = 19, p < 0.01) when compared to LA saline-treated WC (p > 0.05; Fig. 3A and B) and s-GO effect was lost when delivered outside the LA, in the close-by perirhinal cortex (P > 0.05; Fig. 3B). To evaluate the effective ability of s-GO to remove long-term aversive memory and thus PTSD-associated behavior in WC upon s-GO injections, we quantified rat behavior in UC, WC saline and WC s-GO, using the elevated plus maze (EPM) and open field (OF) apparatus (Fig. 3B).

We quantified PTSD-like behavior by measuring the anxiety index in the EPM. WC rats, injected with saline, exhibited a significantly higher (F (91,20) = 0.88, p < 0.05) anxiety index 6 days after the exposure to the predator odor respect to that of UC (saline treated) group. On the contrary, s-GO microinjection into LA reduced the PTSD related behavior in WC animals, decreasing the anxiety index in a statistically significant manner (F (1,20) = 13.43, p < 0.01), if compared to that of the WC saline treated rats. In addition, WC rodents treated with s-GO did not differ from UC (saline or sGO injected) animals (Fig. 3B). We ruled out mere alterations in animal locomotion due to s-GO by testing locomotor behavior *via* the OF apparatus (p > 0.05; Fig. 3B).

3.2. s-GO flakes decrease the activity of glutamatergic synapses in the LA

Suggested molecular mechanisms of the fear components that underlie PTSD include synaptic long-term potentiation (LTP) in LA glutamatergic synapses [44]. We hypothesize that s-GO, once injected in the LA, transiently impair local excitatory glutamatergic synapses, as
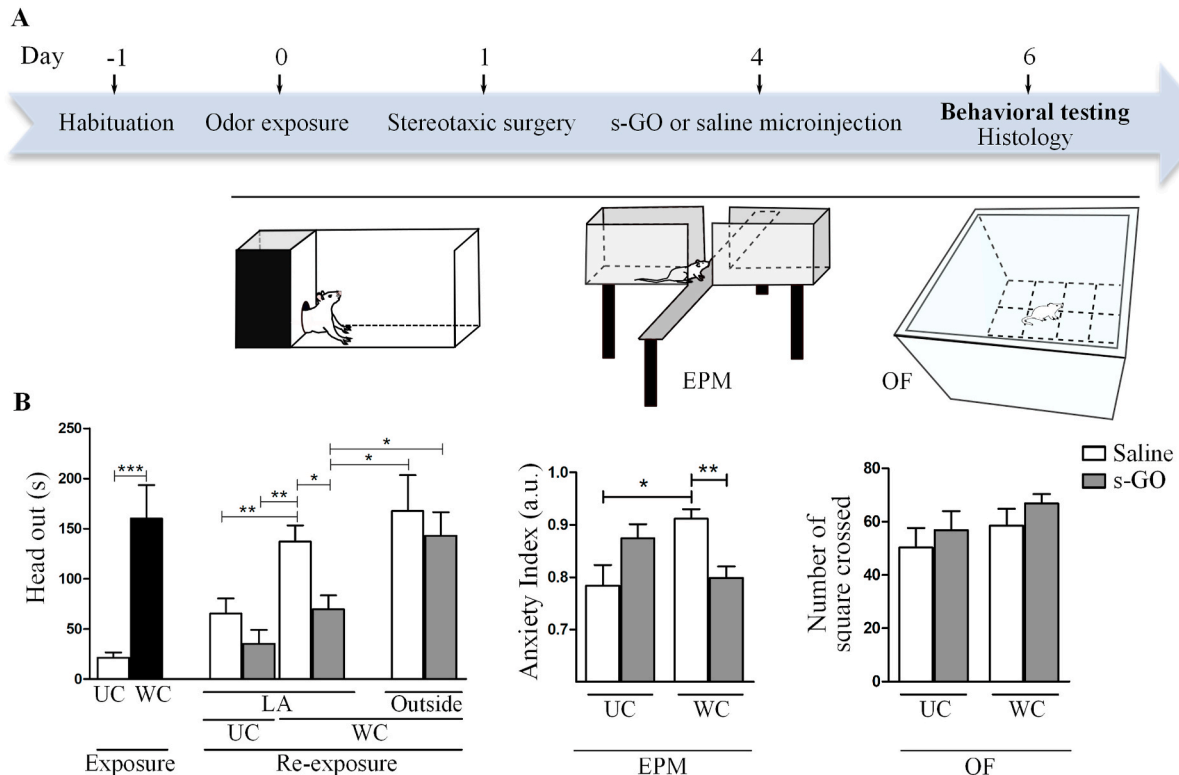

Fig. 3. s-GO delivery in LA impairs long-term fear memories. (A) Schematic representation of the experimental timeline and behavioral testing (at day 6). (B) On the left, bar plot summarizing the head out behavioral responses evoked by the exposure to UC or WC and by the re-exposure to the context after s-GO or saline microinjections into either the lateral amygdala (LA) or the perirhinal cortex. In the middle, bar plot showing the anxiety index evaluated in the EPM test in UC and WC treated with s-GO or saline. On the right, bar plot reporting OF test in UC and WC treated with s-GO or saline. N = 6 for each group. ***p < 0.001; **p < 0.01; *p < 0.05.
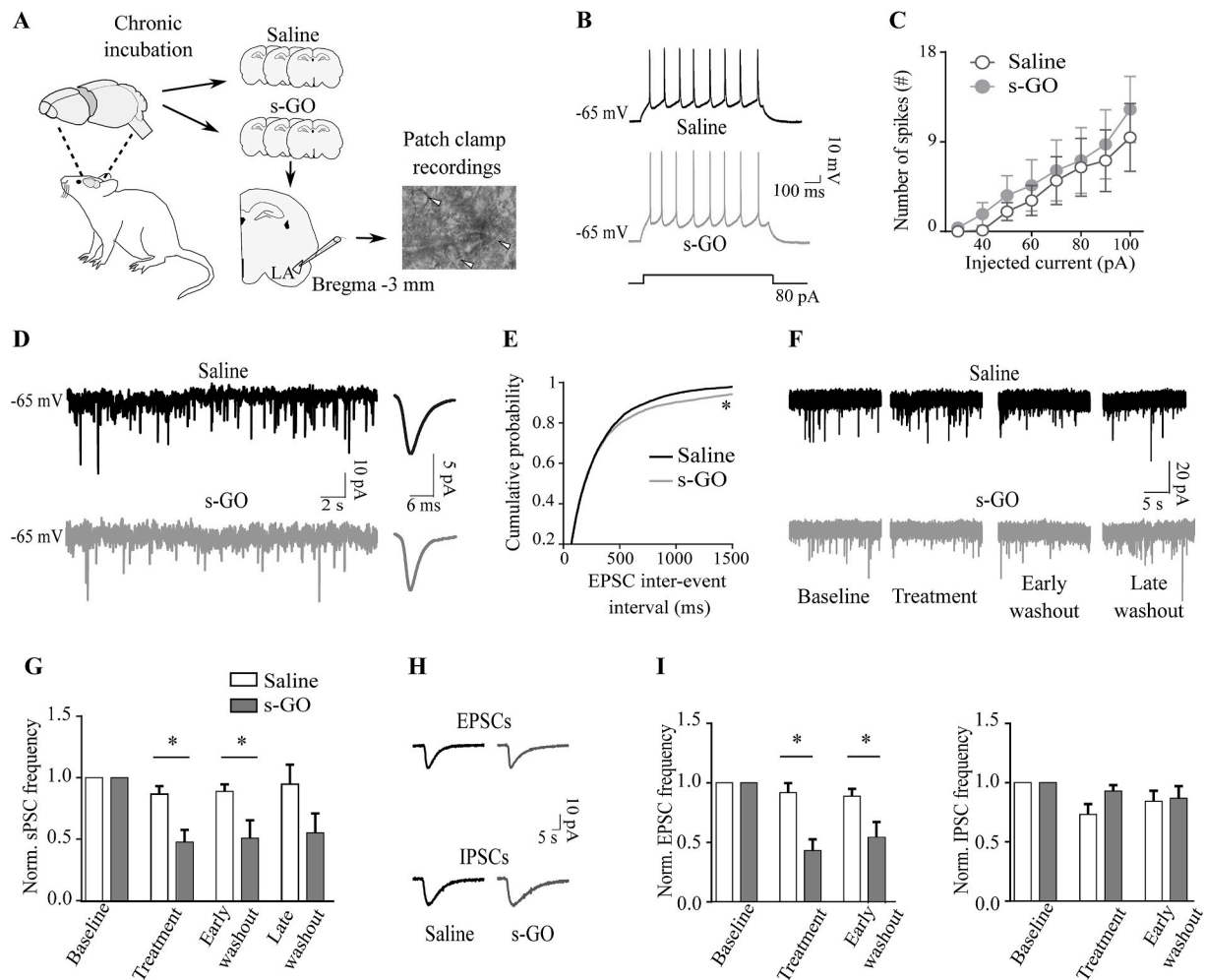
Fig. 4. s-GO downregulate the activity of glutamatergic synapses in the LA (A) Sketch of the experimental settings. (B) Current clamp traces of elicited firing activity in control neurons and in s-GO treated ones. (C) Plot reporting the number of APs fired versus the current injected, for saline-treated (n = 9) and s-GO-treated cells (n = 8). (D) On the left, voltage clamp traces of spontaneous EPSCs recorded in the presence of gabazine (10 μM) in control neurons and s-GO treated ones. On the right, averaged EPSCs waveforms (same cells as left). (E) Cumulative probability plot of the inter event interval of EPSCs for control and s-GO treated neurons: s-GO shift the curve toward larger values. (F) Voltage clamp recordings of sPSCs during acute application of s-GO (n = 9 cells) or saline as control (n = 8 cells) through the perfusion system. Note the downregulation of neuronal activity in s-GO treated cell, while no effect was observed in control. (G) Bar plot showing the statistically significant decrease in normalized sPSCs frequency in s-GO treated cells respect to controls. (H) Averaged EPSCs and IPSCs (same cells as in G) isolated offline on the basis of their different decay times. (I) Bar plots of normalized EPSCs and IPSCs frequency showing that s-GO affect specifically excitatory synapses. Normalized EPSC frequency was decreased (p = 0.0016) during the treatment and during the early phase of the wash out (p = 0.036). Diversely, the normalized IPSCs frequency was not changed by s-GO application.

observed in previous studies [18,19]. Thus, mechanistically, s-GO reduction in glutamatergic synaptic efficacy might prevent LTP expression, crucial to PTSD development. We challenged this hypothesis by single cell electrophysiology *in vitro*. We first incubated acute brain explants containing the amygdala complex with saline or s-GO (50 μg/mL, in saline, 5 h; sketched in Fig. 4A). Under current clamp mode, a homogeneous population of neurons was recorded, identified by their passive (see methods and Table S2) and active (Table S2, Fig. 4B and C) membrane properties, which were not altered by s-GO treatments.

In voltage clamp mode the inter-event interval of spontaneous excitatory glutamatergic postsynaptic currents (EPSCs), pharmacologically isolated in the presence of gabazine (10 μM; see methods and Fig. 4D) were increased after s-GO treatments (432 ± 10 ms) in respect to controls (326 ± 5 ms; see cumulative plot in Fig. 4E; P value < 0.0001). This finding suggests that LA ex-vivo slices, upon prolonged exposure to s-GO [18], displayed a downregulation of glutamatergic transmission. To gain more insights on s-GO dynamics, we administered the nanomaterial acutely (10 μg/mL, 5 min) to the amygdala brain explants while monitoring heterogeneous spontaneous post synaptic

currents (sPSCs) in the absence of pharmacological blockers. Fig. 4F–G shows that s-GO significantly reduced sPSCs frequency when compared to saline (for saline: 0.87 ± 0.06 and for s-GO: 0.47 ± 0.09 Hz; p = 0.0053) and this reduction was maintained during the early phase of s-GO removal (for saline: 0.89 ± 0.06 Hz; and for s-GO: 0.51 ± 0.14; p = 0.0297), with a partial recovery after 10 min washout (for saline: 0.95 ± 0.16 and for s-GO: 0.55 ± 0.16; p > 0.05). Fig. 4H–I shows that in the same experimental conditions, s-GO specifically targeted EPSCs and was ineffective on inhibitory $GABA_A$ receptor mediated postsynaptic currents (IPSCs), identified by their kinetic properties (shown in Fig. 4H, EPSCs displayed typical fast ~5 ms day, while IPSCs featured a slower ~13 ms one [18]) and pharmacology (10 μM CNQX readily abolished fast event, while 10 μM gabazine removed slow ones). Such analysis confirmed that the effect of s-GO in LA tissue was specific for glutamatergic synapses [18,19].

3.3. In vitro long-term potentiation of amygdala synapses is impaired by s-GO

The rescue of anxiety related behaviors observed in animals injected with s-GO hinted at the nanomaterial interference with the building up of the pathological LTP induced by the odor exposure [45]. To explore this possibility, we adopted a simplified *in vitro* model of LTP induction in the amygdala, which allows direct experimental control and access to glutamatergic synapses. We induced synaptic plasticity in dissociated amygdala cultures (Fig. 5A–C) by coupling a brief (30 s) application of glutamate (50 μM) with a depolarization (+4 mV) of the neuronal membrane, favoring the activation of glutamate NMDA receptors, involved in LTP induction [46,47]. Such a treatment resulted in a 30 min long lasting and stable increase in the amplitude of EPSCs (identified by their kinetic properties, voltage dependence and pharmacology, as shown in the Supplementary Figure 2) in respect to the baseline values, while in the controls, that underwent to membrane depolarization in the absence of glutamate application, no changes were detected (normalized amplitudes were 0.81 ± 0.09 in controls, n = 14; 1.72 ± 0.21 in glutamate treated cells, n = 20; p = 0.0004, Fig. 5B–D, 30 min). s-GO (20 μg/mL, 30 s) applied simultaneously to glutamate, blocked the EPSC potentiation (p = 0.0007, Fig. 5C–D). EPCSs frequency remained unaltered in all treatments (Fig. 5E). IPSCs amplitude (Fig. 5 D) and frequency (Fig. 5E) were not modulated by these treatments.

These findings indicate that s-GO target specifically glutamatergic synapses in LA and further suggest that, when applied in conjunction with the LTP inducing stimuli, s-GO may prevent the development of glutamatergic synaptic plasticity.

4. Discussion

We describe here the efficacy of s-GO in preventing the reinforcement of aversive memory and the development of long-term anxiety behavior only when targeting synapses in the LA. We propose that this effect is due to the ability of s-GO to transiently inhibit glutamatergic activity in LA excitatory circuits in a synapse-specific and localized manner, ultimately preventing the emergence of LA dysfunctional plasticity.

We used a widely accepted [36,37] animal model of PTSD. This model is characterized by a correlation between hyperactivity in the LA glutamatergic circuitry and the emergence of anxiety disorders [39,48]. In our experiments, the aversive stimulus induced an innate fear response, measured as an increase in the head out behavior [49]. The rat maintenance of such a behavior when re-exposed to the cat odor-associated context (i.e. neutral environment) [49] supported the fear memory consolidation and, in animals tested six days after the first exposure to the stressful event, the development of long lasting anxiety, as indicated by the EPM test [42]. Long-term aversive memory and the development of long-term anxiety, evoked by a predator odor stress, represent a model of PTSD [50]. In PTSD patients an involvement of amygdala subregion dysfunctional connectivity has been reported [51], accordingly, in the experimental PTSD rat model, neuronal circuitry in the LA undergoes to a reshaping of excitatory glutamatergic synapses [52] featuring the progressive building up of LA synaptic potentiation [53]. Such a boosted excitatory neuronal activity is proposed to trigger the long-term anxiety related behavior [54].

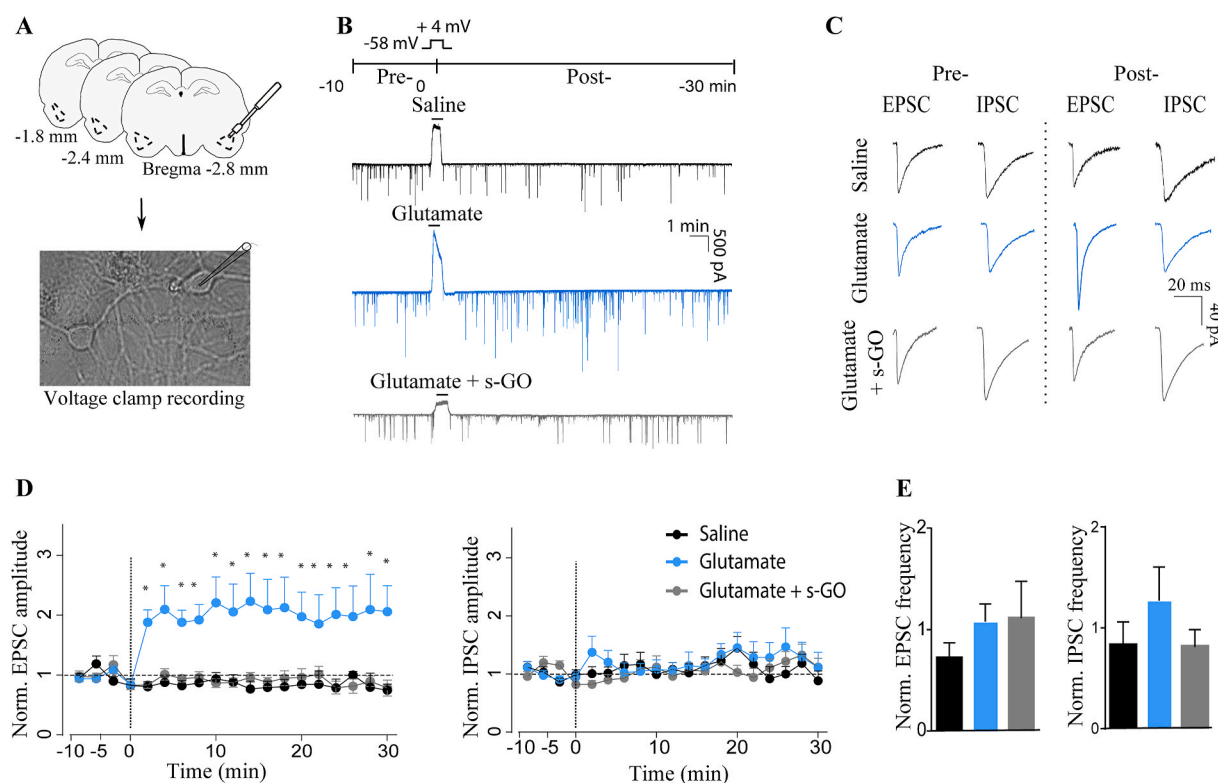s-GO has been reported to specifically interact with glutamatergic

Fig. 5. s-GO impair the long-term potentiation of amygdala synapses *in vitro*. (**A**) Schematic representation of amygdala dissociated cultures and bright field image of cultured cells. (**B**) Representative traces of neuronal spontaneous synaptic activity showing LTP induction in amygdala cultures and its impairment upon s-GO treatment. Chemical LTP was obtained by coupling the depolarization of postsynaptic membrane potential with the application of glutamate at the concentration of 50 μM for 30 s (n = 20 cells). In s-GO treated cells, the nanomaterial was applied together with glutamate under the same condition (n = 17 cells), while control cells were perfused with saline (n = 14 cells). Note the lack of potentiation in s-GO treated cell. (**C**) Offline analysis of sPSCs isolated EPSCs and IPSCs, before and after the treatments. Note that only upon glutamate treatment there is a potentiation of neuronal activity detectable as an increment of the EPSCs amplitude. (**D**) Plots showing that s-GO treatment blocks the 30 min long lasting increase in EPSCs amplitude, observed in neurons undergone to the LTP induction protocol. (**E**) Bar plots showing that the frequency of EPSCs or IPSCs was not affected either by LTP induction or s-GO application. *p < 0.05.

synapses in the CNS inducing a downregulation of excitatory neuro-transmission when applied chronically *in vitro* at a concentration of 10 μg/mL [55] or delivered *in vivo* in one single application at a higher dose. [18,19] *In vivo* s-GO inhibition of glutamatergic synapses in the spinal cord modulates motor behavior [19] and in the rat hippocampus local delivery of s-GO significantly and selectively sized down gluta-matergic activity for 48 h, without altering neuronal viability [18]. In that study, we explored the time course of s-GO fate, which was found to match the synaptic silencing reversibility [18]. Based on these previous evidences, we injected a single dose of s-GO in the LA four days after the exposure to the cat odor to impair glutamatergic transmission for 48 h and eventually interrupt the building up of glutamatergic synaptic plasticity. Indeed, the presence of s-GO in the treated amygdala at 48 h post injection was confirmed and s-GO treatment was effective in dis-rupting both long term aversive memory and anxiety related behaviors. We ruled out potential s-GO nonspecific effects, in fact anxiety responses were unperturbed after 48 h of s-GO delivery outside the LA. In addition, we never detected motor alterations in s-GO treated animals, potentially affecting nonspecifically rat defensive behavior. In this framework, also a generic impact of the surgery procedure or an increased tissue reac-tivity brought about by s-GO injections and affecting synaptic rein-forcement, were excluded.

We adopted *in vitro* amygdala models to experimentally test the mechanistic interaction between s-GO and excitatory synapses. In acute amygdala slices we confirmed that chronic (mimicking *in vivo* accu-mulation) or sub-acute (mimicking *in vivo* diffusion) exposures to s-GO both resulted in a specific reduction in EPSCs frequency, leaving IPSCs unchanged, in accordance to previous reports where s-GO was tested in different CNS areas [18,19,55]. s-GO has been suggested to target pre-synaptic glutamate release in the hippocampus [18], a feature in prin-ciple enabling the alteration of presynaptic mechanisms and glutamatergic transmission engaged in LTP. We further tested in cultured amygdala circuits [33] whether s-GO could impair gluta-matergic synaptic potentiation. We successfully potentiated EPSCs by chemical LTP paradigm (cLTP) [46,56–58] and the application of s-GO during cLTP induction counteracted the synaptic potentiation. Although we cannot demonstrate that *in vivo* s-GO prevented the potentiation of amygdala circuits usually linked to PTSD development [44], it is tempting to speculate that the injection of s-GO in the LA during a temporal window crucial to the reinforcement of plastic changes related to the contextual fear memory acquisition [38], effectively reduced glutamatergic transmission potentiation and the onset of downstream long lasting anxiety-related behavior. s-GO nanoflakes might therefore be clinically exploited in the broader area of engineered nanoparticles for precision-medicine applications [59], to allow improved sub-cellular (*i.e.* synaptic) targeting in neurological disorders.

5. Conclusion

Our experiments suggest that s-GO nanoflakes, thanks to their action as synaptic and behavioral modulators, might effectively hinder path-ological behaviors based on aberrant glutamatergic transmission.

Author contributions

AFB and NCC designed the PTSD paradigm; AFB performed the behavior, surgery and histology; RC performed confocal microscopy; GC designed the electrophysiology; GC and EP performed the electrophys-iology; AFB, GC and EP analyzed data; NL, BB and KK design, produced and characterized materials; LB conceived the idea, designed research and wrote the MS.

Declaration of competing interest

The authors declare that they have no known competing financial interests or personal relationships that could have appeared to influence the work reported in this paper.

Appendix A. Supplementary data

Supplementary data to this article can be found online at https://doi.org/10.1016/j.biomaterials.2021.120749.

Data and materials availability

The data that support the findings of this study are available from the corresponding authors upon reasonable request.

References

[1] E.R. Duval, J. Sheynin, A.P. King, K.L. Phan, N.M. Simon, B. Martis, K.E. Porter, S. B. Norman, I. Liberzon, S.A.M. Rauch, Depress. Anxiety 37 (2020) 670–681.
[2] A.L. Gold, R. Abend, J.C. Britton, B. Behrens, M. Farber, E. Ronkin, G. Chen, E. Leibenluft, D.S. Pine, Am. J. Psychiatr. 177 (2020) 454–463.
[3] J.E. Hassell Jr., K.T. Nguyen, C.A. Gates, C.A. Lowry, Curr Top Behav Neurosci 43 (2019) 271–321.
[4] N.C. Coimbra, T. Paschoalin-Maurin, G.S. Bassi, A. Kanashiro, A.F. Biagioni, T. T. Felippotti, D.H. Elias-Filho, J. Mendes-Gomes, J.P. Cysne-Coimbra, R.C. Almada, B. Lobão-Soares, Rev. Bras. Psiquiatr. 39 (2017) 72–83.
[5] P. Tovote, J.P. Fadok, A. Lüthi, Nat. Rev. Neurosci. 16 (2015) 317–331.
[6] D. Busti, R. Geracitano, N. Whittle, Y. Dalezios, M. Mańko, W. Kaufmann, K. Sätzler, N. Singewald, M. Capogna, F. Ferraguti, J. Neurosci. 31 (2011) 5131–5144.
[7] R.K. Butler, A.C. Sharko, E.M. Oliver, P. Brito-Vargas, K.F. Kaigler, J.R. Fadel, M. A. Wilson, Bone 23 (2011) 133–144.
[8] S. Duvarci, D. Pare, Neuron 82 (2014) 966–980.
[9] M.P. Parsons, L.A. Raymond, Neuron 82 (2014) 279–293.
[10] D.M. Bannerman, R. Sprengel, D.J. Sanderson, S.B. Mchugh, J.N.P. Rawlins, H. Monyer, P.H. Seeburg, Nat. Rev. Neurosci. 15 (2014) 181–192.
[11] L. Musazzi, G. Racagni, M. Popoli, Neurochem. Int. 59 (2011) 138–149.
[12] J.-Y. Zhang, T.-H. Liu, Y. He, H.-Q. Pan, W.-H. Zhang, X.-P. Yin, X.-L. Tian, B.-M. Li, X.-D. Wang, A. Holmes, T.-F. Yuan, B.-X. Pan, Biol. Psychiatr. 85 (2019) 189–201.
[13] A.K. Geim, K.S. Novoselov, Nat. Mater. 6 (2007) 183–191.
[14] L. Feng, L. Wu, X. Qu, Adv. Mater. 25 (2013) 168–186.
[15] G. Yang, J. Su, J. Gao, X. Hu, C. Geng, Q. Fu, J. Supercrit. Fluids 73 (2013) 1–9.
[16] K. Kostarelos, M. Vincent, C. Hebert, J.A. Garrido, Adv. Mater. 29 (2017) 1–7.
[17] M. Bramini, G. Alberini, E. Colombo, M. Chiacchiaretta, M.L. DiFrancesco, J. F. Maya-Vetencourt, L. Maragliano, F. Benfenati, F. Cesca, Front. Syst. Neurosci. 12 (2018) 1–22.
[18] R. Rauti, M. Medelin, L. Newman, S. Vranic, G. Reina, A. Bianco, M. Prato, K. Kostarelos, L. Ballerini, Nano Lett. 19 (2019) 2858–2870.
[19] G. Cellot, S. Vranic, Y. Shin, R. Worsley, A.F. Rodrigues, C. Bussy, C. Casiraghi, K. Kostarelos, J.R. McDearmid, Nanoscale Horizons 5 (2020) 1250–1263.
[20] H. Ali-Boucetta, D. Bitounis, R. Raveendran-Nair, A. Servant, J. Van den Bossche, K. Kostarelos, Adv. Healthc. Mater. 2 (2013) 433–441.
[21] D.A. Jasim, N. Lozano, K. Kostarelos, 2D Mater. 3 (2016), 014006.
[22] S.P. Mukherjee, N. Lozano, M. Kucki, A.E. Del Rio-Castillo, L. Newman, E. Vazquez, K. Kostarelos, P. Wick, B. Fadeel, PLoS One 11 (2016), e0166816.
[23] A.F. Rodrigues, L. Newman, D.A. Jasim, I.A. Vacchi, C. Ménard-Moyon, L.E. Crica, A. Bianco, K. Kostarelos, C. Bussy, Arch. Toxicol. 92 (2018) 3359–3379.
[24] H. Cohen, J. Zohar, Z. Kaplan, J. Arnt, Eur. Neuropsychopharmacol 28 (2018) 63–74.
[25] J. Tejada, K.T. Chaim, S. Morato, Psicol. Teor. Pesqui. 33 (2017) e3322.
[26] G. Paxinos, C.R. Watson, The Rat Brain in Stereotaxic Coordinates, sixth ed., Elsevier Academic Press, San Diego, 2007.
[27] A.F. Biagioni, R.C. de Oliveira, R. de Oliveira, J.A. da Silva, T. dos Anjos-Garcia, C. M. Roncon, A.P. Corrado, H. Zangrossi, N.C. Coimbra, Eur. Neuropsychopharmacol 26 (2016) 532–545.
[28] M. Musto, R. Rauti, A.F. Rodrigues, E. Bonechi, C. Ballerini, K. Kostarelos, L. Ballerini, Front. Syst. Neurosci. 13 (2019) 1–15.
[29] E.L. Louth, C.D. Sutton, A.L. Mendell, N.J. Maclusky, C.D.C. Bailey, JoVE 122 (2017), e55358.

[30] W.C. Risher, T. Ustunkaya, J.S. Alvarado, C. Eroglu, PloS One 9 (2014), e107591.
[31] P. Chakraborty, S. Chattarji, Psychopharmacology 236 (2019) 73–86.
[32] R. Mitra, R. Adamec, R. Sapolsky, Behav. Pharmacol. 205 (2009) 535–543.
[33] N. Secomandi, A. Franceschi Biagioni, K. Kostarelos, G. Cellot, L. Ballerini, Nanomed. Nanotechnol. Biol. Med. 26 (2020) 102174.
[34] R. Khazipov, D. Zaynutdinova, E. Ogievetsky, G. Valeeva, O. Mitrukhina, J. B. Manent, A. Represa, Front. Neuroanat. 9 (2015) 1–5.
[35] J.P. Johansen, H. Hamanaka, M.H. Monfils, R. Behnia, K. Deisseroth, H.T. Blair, J. E. LeDoux, Proc. Natl. Acad. Sci. U. S. A 107 (2010) 12692–12697.
[36] R.A. Dielenberg, G.E. Hunt, I.S. McGregor, Neuroscience 104 (2001) 1085–1097.
[37] L.K. Takahashi, B.R. Nakashima, H. Hong, K. Watanabe, Neurosci. Biobehav. Rev. 29 (2005) 1157–1167.
[38] N.S. Canteras, E. Pavesi, A.P. Carobrez, Front. Neurosci. 9 (2015) 1–10.
[39] J.A. Rosenkranz, E.R. Venheim, M. Padival, Biol. 67 (2010) 1128–1136.
[40] L.G. Staples, I.S. McGregor, R. Apfelbach, G.E. Hunt, Neuroscience 151 (2008) 937–947.
[41] A. Berardi, V. Trezza, M. Palmery, L. Trabace, V. Cuomo, P. Campolongo, Front. Behav. Neurosci. 8 (2014) 1–12.
[42] C. Muñoz-Abellán, R. Andero, R. Nadal, A. Armario, Psychoneuroendocrinology 33 (2008) 1139–1150.
[43] R.C. Martinez, E.F. Carvalho-Netto, É.R. Ribeiro-Barbosa, M.V.C. Baldo, N. S. Canteras, Neuroscience 172 (2011) 314–328.
[44] A.L. Mahan, K.J. Ressler, Trends Neurosci. 35 (2012) 24–35.
[45] K.J. Wallace, J.B. Rosen, J. Neurosci. 21 (2001) 3619–3627.
[46] A. Malgaroli, R.W. Tsien, Nature 357 (1992) 134–139.
[47] R.J. Cormier, P.T. Kelly, J. Neurophysiol. 75 (1996) 1909–1918.
[48] H.T. Blair, G.E. Schafe, E.P. Bauer, S.M. Rodrigues, J.E. LeDoux, Learn. Mem. 8 (2001) 229–242.
[49] I.S. McGregor, L. Schrama, P. Ambermoon, R.A. Dielenberg, Behav. Brain Res. 129 (2002) 1–16.
[50] M.A. Matar, H. Cohen, Z. Kaplan, J. Zohar, Neuropsychopharmacology 31 (2006) 2610–2618.
[51] D. Rabellino, M. Densmore, P.A. Frewen, J. Théberge, M.C. McKinnon, R.A. Lanius, PloS One 11 (2016), e0163097.
[52] B.M. Sharp, Transl. Psychiatry 7 (2017) e1194.
[53] J.P. Johansen, C.K. Cain, L.E. Ostroff, J.E. LeDoux, Cell 147 (2011) 509–524.
[54] O. Babaev, C. Piletti Chatain, D. Krueger-Burg, Exp. Mol. Med. 50 (2018) 1–16.
[55] R. Rauti, N. Lozano, V. León, D. Scaini, M. Musto, I. Rago, F.P. Ulloa Severino, A. Fabbro, L. Casalis, E. Vázquez, K. Kostarelos, M. Prato, L. Ballerini, ACS Nano 10 (2016) 4459–4471.
[56] R.J. Cormier, M.D. Mauk, P.T. Kelly, Neuron 10 (1993) 907–919.
[57] A. Louveau, J. Angibaud, F. Haspot, M.C. Opazo, R. Thinard, V. Thepenier, S. J. Baudouin, L. Lescaudron, P. Hulin, C.A. Riedel, H. Boudin, J. Neurosci. 33 (2013) 18672–18685.
[58] M. Kintscher, C. Wozny, F.W. Johenning, D. Schmitz, J. Breustedt, Nat. Commun. 4 (2013) 1–8.
[59] M.J. Mitchell, M.M. Billingsley, R.M. Haley, M.E. Wechsler, N.A. Peppas, R. Langer, Nat. Rev. Drug Discov. 20 (2020) 101–124.